Nanofluidic interfaces in microfluidic networks

Running title: Fabrication of Nanofluidics within Microfluidics

Running Authors: Millet et al.

Larry J. Millet [a)]

Biosciences Division and The Center for Nanophase Materials Sciences, Oak Ridge National Laboratory, Oak Ridge, TN 37831, USA

Mitch J. Doktycz

Biosciences Division and The Center for Nanophase Materials Sciences, Oak Ridge National Laboratory, Oak Ridge, TN 37831, USA

Scott T. Retterer

Biosciences Division and The Center for Nanophase Materials Sciences, Oak Ridge National Laboratory, Oak Ridge, TN 37831, USA

[a)] Electronic mail: milletlj@ornl.gov

The integration of nano- and microfluidic technologies enables the construction of tunable interfaces to physical and biological systems across relevant length scales. The ability to perform chemical manipulations of miniscule sample volumes is greatly enhanced through these technologies and extends the ability to manipulate and sample local fluidic environments at subcellular, cellular and community or tissue scales. Here we describe the development of a flexible surface micromachining process for the creation of nanofluidic channel arrays integrated within SU-8 microfluidic networks. The use of a semi-porous, silicon rich, silicon nitride structural layer allows for a rapid removal of the sacrificial silicon dioxide during the nanochannel fabrication.

Nanochannel openings that form the interface to biological samples are customized using focused ion beam milling. The compatibility of these interfaces with on-chip microbial culture is demonstrated.

I. INTRODUCTION

Chemical signatures in biological systems are dynamic and span intra- and inter-cellular domains with length-scales from nanometers to meters. Resolving spatiotemporal dynamics of these signatures is a grand challenge in environmental and ecological sciences and is fundamental to understanding complexity in biological systems.[1-3] Presently, spectroscopic and spectrometric measurement techniques are unable to directly resolve chemical distributions at the subcellular scale. Chemical signatures that vary rapidly with fluctuations in the concentrations of multiple molecular species are particularly difficult to resolve.[4-7] Solving problems of chemical access and measurement to meet this challenge requires the advancement of nano- and microfabrication processes to enable chemical measurement and detection strategies.[8]

Nano- and microfluidic technologies can play a crucial role in enabling the interrogation and manipulation of complex biological systems across scales, from the subcellular, to cellular, and within multicellular ensembles. Dynamic maps of chemical signatures are typically inaccessible with conventional technologies. Prokaryotes and eukaryotic systems interact through chemical and physical means for cooperation, competition, or conflict. Microfluidics and surface patterning of synthetic environments, allow for precise definition of physicochemical properties,[9-12] for the characterization of cellular and molecular interactions,[13-16] developmental requirements,[17] and mechanisms

of emergent behaviors.[18] Integrated fluidics provide potential advancements in chemical sampling strategies; when combined with structures for molecular capture, nano- and microfluidics can be used to access and route chemical information[19-23] while facilitating the exchange of energy and materials.[24-26] This work describes the development of a broad-use fluidic platform that enables the routing of chemical information (*e.g*. auxins, N-Acyl homoserine lactones, indoleacetic acid, etc) to and/or from subregions of a biological specimen (*e.g*. adherent biofilms or cell populations) for subsequent chemical analyses. Fluidic channels ranging from nanometers to micrometers meet scaling requirements for dosing or sampling prokaryotic and eukaryotic specimens from the subcellular scale through the level of functional multicellular communities and tissues (*e.g*. biofilms, tissue culture, neural networks).

Here, surface micromachining techniques[27] were used to define nanofluidic architectures; processes used include electron beam lithography, plasma-enhanced vapor-phase deposition of silicon-dioxide (sacrificial layer), reactive ion etching, ion milling, photolithography, plasma oxidation, and thermal annealing.[28-31] The internal structures of nanochannels are cleared of the sacrificial silicon dioxide to form silicon-rich silicon-nitride nanochannels. The fluidic cavity is verified through ion milling and scanning electron microscopy. Nanochannel inlets and outlets were selectively opened using focused ion beam milling. This creates a tailored nanofluidic interface that spans between microfluidic channels in which bacterial growth, microbial community development, and sample collection/concentration can be performed. In the current platform, diffusion is likely to dominate material exchange across the nanochannels. Additional insulation and

surface patterned electrodes can be readily incorporated into the device design to facilitate electrokinetic control of fluid flow and mass transport.

II. EXPERIMENTAL

A nanofluidic interface was formed using silicon micromachining processes and then integrated within a SU-8 and PDMS microfluidic network (Fig. 1). These processes yield a biocompatible platform that enables bacterial cultures at ion-milled nanofluidic interfaces.

A. PECVD Deposition of Sacrificial Oxide

Silicon wafers (<100>, p-type, 500 μm) were used for the starting material. A sacrificial silicon dioxide thin film was deposited by plasma enhanced chemical vapor deposition (PECVD) (Oxford Plasmalab 100 PECVD System, Abington, Oxfordshire, UK) (Fig. 1A). Deposition was carried out at 350^{o}C under a flow of 5% SiH_4/Ar at 170sccm and N_20 at 710sccm. The chamber was maintained at a pressure of 1000mT with a forward RF power of 20 W for 8 minutes and 15 seconds. The thickness measured by interferometry and later verified by scanning electron microscopy was nominally 500nm. Prior to sample deposition, a 5 minute deposition on a 'dummy' sample was used to condition the chamber.

B. E-beam Lithography

For nanolithography, a high performance electron-beam resist, ZEP520A (ZEON, Tokyo, Japan), was spin-coated at 1000 rpm to a nominal thickness of 500 nm onto the silicon wafers and baked at 180 °C for 120 sec. Wafers were patterned with a JEOL USA JBX-9300FS Electron Beam Lithography system (Peabody, MA) with exposure settings of 2 nA, 4 nm shot pitch, and a dose of 400 μC/cm^2. Following exposure, wafers were developed in xylenes for 20 seconds, immediately rinsed with IPA and dried with

purified nitrogen. Exposure in a small area around the nanochannels (75 μm to 90 μm, length), was performed leaving resist covering the majority of the wafer and the narrow lines that mask the oxide that ultimately forms the interior of the nanochannels (Fig. 1B).

C. Reactive Ion Etching of the Sacrificial Oxide

The sacrificial oxide was etched from exposed regions of the wafer using a reactive ion etch (RIE) (Oxford Instruments Plasmalab 100 RIE/ICP Etcher, Abington, Oxfordshire, UK). The oxide etch applies 200 W forward RF power and 2000 W ICP power to a flow of C_4F_8 at 45.0 sccm and O_2 at 2.0 sccm in a chamber with pressure of 7.0 mT and temperature of 15 °C. The RIE process was carried out until the silicon dioxide was completely removed from the exposed areas, approximately 165 seconds (Fig. 1C). The resist etch mask was removed in an n-methyl pyrrolidinone (NMP) bath at 70 °C.

D. PECVD Deposition of Silicon Nitride

Deposition of a silicon-rich, ammonia-free silicon nitride thin film that is highly resistant to HF etching was achieved by plasma-enhanced chemical vapor deposition (Oxford Plasmalab 100 PECVD System). Pre-conditioning of the chamber (ran with a dummy wafer 400 ^{o} C, 30 min) was performed prior to deposition. Wafers with patterned oxide were heated to 400 ^{o}C and exposed for 7 min 15 sec to a flow of 5% SiH_4/Ar at 150 sccm and N_2 at 790 sccm at a chamber pressure of 1200 mT and forward RF power of 60 W to produce a silicon-rich silicon nitride layer approximately 365 nm thick (Fig. 1D). Thickness was estimated based on empirical deposition rates and verified by SEM.

E. Patterning of Nanochannel Outlets and Oxide Removal

Conventional contact lithography was used to pattern a photoresist etch mask. Briefly, MicroPrime P20 adhesion promoter (Shin-Etsu Microsci, Phoenix, AZ) was spin coated on the wafer, left for 10s and spin dried at 3000 rpm for 45s. Megposit™ SPR™220 4.5 (Micro-Chem) was spin-coated at 3000 rpm and baked at 90^{o}C for 90 seconds. The resist was exposed for 13 seconds in pressure-contact, post-exposure baked for 60 seconds at 115^{o}C, and developed in aqueous tetramethyl ammonia hydroxide developer (<2%) for one minute. An area tracing the entire outer edge of the initial electron beam lithography (EBL) pattern, overlapping the ends of the oxide channels, was exposed, creating a small 'bow-tie' cut out of the nanochannel array. To expose the underlying sacrificial oxide, a 45 sec RIE etch was performed as specified (Ar = 1.5 ccm, SF6 = 45 sccm, 10 mT chamber pressure at 5 ^{o}C, 50 W RF power, and 2000 W ICP power). Once access to channels was created by RIE, the samples were exposed to 49% HF for 1.0 min at ~22-25 ^{o}C to remove the sacrificial oxide (Fig. 1E). Because of the semi-porous nature of the silicon rich nitride, the silicon nitride lying atop the sacrificial oxide (with the exception of the nanofluidic channels) was also removed during this process.

F. Patterning of SU-8 Fluid Networks

Details for in-house photomask patterning have been described in previous work.[32] Masks were cleaned prior to use by rinsing with deionized water and drying with nitrogen. For open microchannels aligned to nanochannels, the patterns were formed with SU-8 2015 spin-coated at 6000 rpm to a thickness of 10 µm, then soft-baked at 95°C, for 4 min, and exposed for 6 sec with 365-nm light. Samples were baked at 95°C for 5 min

and developed until clear (SU-8 developer). A final hard bake was carried out for 5 minutes at 180 °C (Fig. 1F).

G. Ion Beam Milling

Prior to ion milling, a thin chromium layer (~10nm) was deposited via electron beam evaporation to prevent SU-8 charging during imaging. The ion source (30 kV, 50 pA) and electron beam (7.5 kV) (FEI Novalab 600 Dual-Beam (electron/ion)) were used to mill (6,000x) and image (10,000x) the nanochannel surface (Fig. 1G).

H. PDMS Microfluidic Enclosure

Open-channel SU-8 microchannels aligned to nanofluidics were closed through either one of two methods, nitrogen plasma activation and annealing, or by vacuum sealing. For nitrogen plasma activation, a nitrogen (99.99%) gas tank was connected to a plasma generator (Harrick plasma) on high. For vacuum sealing, clean PDMS forms (3-4 mm thick slab) were placed in conformal contact to SU-8 patterned open-channel structures then retained under strong vacuum ($\geq$ 30 min). Upon returning the sample to atmospheric conditions, forceps were used to press the PDMS against the surface of the SU-8. Micro and nanofluidic platforms were left at ambient conditions or $\geq$ 20 min to seal.

I. Bacterial Culture

The BSL2 *Pseudomonas aeruginosa* eGFP strain (attTn7::GFP) was a generous gift from the J. Mougous Laboratory (University of Washington, Seattle, WA). Cultures were grown on Luria Broth (LB) plates and in liquid culture with LB media without antibiotics and according to conventional BSL2 safety practices. The bacterial culture in

microfluidics was achieved with stationary fluid (no flow) cultures overnight at 37 °C without shaking.

IV. RESULTS AND DISCUSSION

Nanofluidic architectures have the promise of enabling biochemical discoveries from biological systems due to the ability to route information, energy, and materials in chemical form. To this end, architectures were designed and patterned according to the process summarized in Figure 1. A combination of surface micromachining and conventional SU-8 photopatterning was used to form a nanofluidic interface within a microfluidic network (Fig. 2A-C). This SU-8 microfluidic platform can be sealed with PDMS to enable biological cultures within this micro and nanofluidic system (Fig. 2D).

The process we employed for micromachining nanofluidic structures makes use of sequential deposition, lithography, and etching to produce silicon-rich nitride nanofluidics. When etching the sacrificial oxide to form the nanofluidic cavity, care must be taken to avoid over etching since the RIE process anisotropically etches the silicon substrate. The silicon-rich nitride appears to allow permeation of the ionic HF etchant, a process that attacks the underlying sacrificial oxide to permit a rapid clearing of the nanochannels and removal of the nitride over large areas that are not in direct contact with the silicon, thus decreasing the time required for removal of the sacrificial oxide from an estimated time of nearly 1 hour to only1-2 min.

Scanning electron micrographs of the ammonia-free silicon-rich silicon nitride (Fig. 3) show the porous nature of the material. The rapid removal of the sacrificial silicon dioxide and associated lift-off of large areas of the silicon nitride suggests that the

silicon nitride is permeable to ions. Prior to nanofluidic dosing and sampling through this silicon-rich nitride surface, the permeability of the silicon nitride structures (*e.g.* channel walls) will need to be determined. This can be accomplished by implementing micro- or nano-fluidic size-exclusion chromatographic techniques or performing molecular filtration and detection of molecular weight standards.[32-34]

The only nitride-coated surface features that were retained on the wafer through the HF etch process were the silicon nitride "bow tie" structures (Fig. 1E, Fig. 2A-B); the bow-tie structures were initially patterned with EBL to define the sacrificial oxide, exposing a larger silicon "bow-tie" area (Fig. 2A,B) The structural silicon-rich nitride layer (*i.e.* the bow ties) was deposited directly onto the entire wafer, and adhered directly to the silicon substrate through the EBL-patterned "bow-tie" windows (Fig. 1 C-E). RIE of a pattern that outlines the edge of the "bow-tie" pattern simultaneously opened the ends of the nanochannels and physically separated the "bow-ties" from the surrounding silicon nitride. This helped to prevent tearing of the silicon nitride adhered to the silicon surface and significantly improved the yield of nanofluidic structures. The rapid silicon nitride "lift-off" of the majority of silicon nitride on the sample was not anticipated, but allowed for a rapid clearing of the channels. This rapid oxide removal process may prove beneficial for microfabrication processes where ion species selectivity is desired or can be tolerated, and short sacrificial oxide removal times are highly desirable.

The exterior surface of the nanochannel presents a characteristic nano-scale surface roughness (Fig. 3) that forms as a result of different material substrates, topology, and heat conduction differences from the elevated channel and the planar silicon background material. The grainy silicon-rich nitride may be beneficial for anchoring

polymeric (*e.g.* SU-8) microfluidics that are formed through photolithography, and may ultimately alter the adhesion of microbial species during culture.

Ion milling was used to (1) open the sealed channel ends, (Fig. 4-5) making the internal cavity of the nanochannel fluidically accessible, and (2) sectioning the nanofluidic channels to verify the formation of an open internal fluidic space following the silicon etch process (Fig. 4-5). The resulting nanochannel dimensions are 75 μm to 90 μm (length), 500 nm (cavity width), and 300 nm (cavity height); the exterior channel width is 1 micron (width).

Because this fabrication process produced raised channels with nanoscopic surface roughness, a conformal process was required to fabricate the microfluidics onto the nanochannels to seal adjacent microfluidic domains from each other. Photolithographically patterned SU-8 resist was used to create microfluidics aligned to the nanochannel arrays (Fig. 5A). As a result, open-channel microfluidic structures provide a smooth surface for channel closure, and when sealed, create compartmentalized microfluidic domains. Conventional PDMS microfluidics cannot be fabricated and aligned to the nanochannels directly as they would leave nanofluidic voids in the corners of the nanochannel base and between the nanoscopic hills and valleys where cured PDMS could not fill. By fabricating SU-8 microchannels directly onto the nanochannel array, defects (*e.g*. particles) are avoided that can produce gaps between PDMS channels and the surface, thus compromising fluidic integrity. Another benefit of direct SU-8 microfluidic fabrication is that contact aligners provide more precise alignment than procedures for aligning pre-fabricated PDMS-based microfluidics. As a result, the

dielectric-to-polymer material integration provides a tight seal between the silicon nitride and the SU-8 microfluidics.

Ion-beam milling is a high precision process that can be used to selectively carve materials and surfaces to nanoscale precision. Here we used ion milling to open the channel ends at the location of biological sampling (Fig. 5B). Depending on the channel architecture, ion milling may be used to create slits or perforations in the nanofluidic structure. Figure 5C shows the results of a two-step milling process that creates a pore into the channel, or may be used to cleave off the channel end to reveal the open fluid space and display the milling profile of the channel pores shown in Figure 5B. Ion milling, while more time consuming, can yield a greater channel opening density than conventional photopatterning allows, furthermore, the size and placement of the openings can be tailored to each experiment.

Micromachined nanofluidic structures integrated within open-channel SU-8 microfluidics were sealed with a thin slab (~3 mm) of PDMS containing integrated tubing segments registered to each port (Fig. 2D). To seal the PDMS slab onto the SU-8 structures, the SU-8 photolithographic pattern was designed with large voids and pillars in the open space between the nano- and microfluidics (Fig. 2D). These voids assist in sealing and holding PDMS in place and prevent PDMS collapse. The pillars prevent PDMS collapse into the intervening void between channels, and the voids (containing SU-8 pillars) assist in holding the plasma-treated PDMS in place through suction. This was achieved by placing a clean, particle-free PDMS slab onto the SU-8 channels, the combined assembly was placed into a vacuum chamber and degassed for 20 min. Upon removing the PDMS-silicon chip from the vacuum system, the PDMS was pressed onto

the SU-8 surface (if not already in contact) to bring the SU-8 and PDMS into conformal contact. At ambient conditions, the PDMS absorbs gas from its surroundings, including the microfluidic voids between the PDMS and the silicon. As the gas becomes depleted from the intervening space (between the SU-8 frame and pillars), a negative pressure builds within this space to hold the PDMS in place through suction. This adhesive suctioning approach combined with PDMS and plasma treatment provides a sufficient force to keep the microfluidic channels sealed for fluidic studies and bacterial cultures. Alternatively, this same process can be performed with vacuum aspiration using pumps to continuously supply suction to the intervening voids and hold the PDMS onto the SU-8 for a reversible seal. This assembly process is compatible with hydrodynamic flow manipulations, and the degassed PDMS also eliminates any air bubbles that are in contact with the PDMS elastomeric slab while trapped in the channel.

Figure 6 shows a completed assembly of a nano- to microfluidic array where 10 channels with SU-8 microfluidics interface with nanochannels. The simplified and compact fluidic architecture is designed for dosing or sampling of a small sub-region of the channel (15 um x 20 um). Benefits to small numbers of channels in close proximity are for the simultaneous observation of chemical transients in one image field at high magnification and temporal sampling from the same region through different channels. Future designs could make use of more distributed and stratified channel spacing for dosing or sampling along the length of the central microfluidic channel. The PDMS sealing approach employed here maintains fluidic integrity between microfluidic compartments (Fig. 6B); air is observed in the 10 terminal SU-8 microfluidic channels while the central culture channel remains filled with fluid (Fig. 6C). As an indication of

microfluidic fidelity of the SU-8 and PDMS channel closure, microbial cultures were maintained overnight (Fig. 6C) then processed for electron microscopic observation (Fig. 6D).

Figure 6D shows a high magnification image of one of the nanofluidic channels with *Pseudomonas aeruginosa* and putative exopolysaccharide streamers on the surface (SEM image). Bacterial exopolysaccharides in culture form stringy smears that appear as "streamers."[35] The bacterial cultures can be grown in the microfluidic channel under stationary conditions overnight. In a microfluidic channel 1 cm (l) x 15 μm (w) x 10 μm (h) there is ample nutrients and volume for bacterial growth (bacteria size = 500 nm (dia.) x ~1 μm (l)) and expansion in overnight culture within a biocompatible microenvironment." The integrated platforms were prepared and processed for scanning electron microscopy, and imaged after removing the PDMS lid. Current work is focused on understanding and controlling transport through the nanofluidic interface. These results demonstrate a process for creating microfluidic and nanofluidic platforms that are accessible through reversible PDMS closures for sample manipulation and subsequent access.

V. SUMMARY AND CONCLUSIONS

Nanofluidic architectures formed through micromachining can be integrated into polymeric microfluidic platforms for reversibly-sealed fluidic assemblies. Semi-porous silicon-rich nitride films enable a rapid lift-off by simultaneous and ubiquitous removal of the underlying sacrificial oxide. These nano and microfluidic platforms allow for

interfacing with biological specimens due to the fluidic scales, reversible tight seals, and biocompatibility.

ACKNOWLEDGMENTS

This manuscript has been authored by UT-Battelle, LLC under Contract No. DE-AC05-00OR22725 with the U.S. Department of Energy. The United States Government retains and the publisher, by accepting the article for publication, acknowledges that the United States Government retains a non-exclusive, paid-up, irrevocable, world-wide license to publish or reproduce the published form of this manuscript, or allow others to do so, for United States Government purposes. The Department of Energy will provide public access to these results of federally sponsored research in accordance with the DOE Public Access Plan(http://energy.gov/downloads/doe-public-access-plan).

This work was supported by Office of Science/Biological and Environmental Research (BER), project number ERKP851. The views expressed are those of the authors and do not reflect the official policy or position of the Department of Defense or the U.S. Government. This research was performed at Oak Ridge National Laboratory (ORNL). ORNL is managed by UT-Battelle, LLC, for the US Department of Energy Under contract DE-AC05-00OR22725. Nanofluidic platforms were fabricated and SEM imaging was performed at the Center for Nanophase Materials Sciences, which is sponsored at Oak Ridge National Laboratory by the Scientific User Facilities Division, Office of Basic Energy Sciences, U.S. Department of Energy.

[1]J. Vacheron, G. Desbrosses, M.-L. Bouffaud, B. Touraine, Y. Moënne-Loccoz, D. Muller, L. Legendre, F. Wisniewski-Dyé, and C. Prigent-Combaret, Front. Plant Sci. **4,** 356, (2013).
[2]J. S. Satterlee, A. Beckel-Mitchener, A. R. Little, D. Procaccini, J. L. Rutter, and A. C. Lossie, Neuroepigenetics. **1**, 2, (2015).
[3]S. Dong, J. A. Allen, M. Farrell, and B. L. Roth, Mol. Biosyst. **6,** 1376, (2010).
[4]L. Nováková and H. Vlčková, Anal. Chim. Act. **656,** 8, (2009).
[5]Y. Zhu and Q. Fang, Anal. Chim. Act. **787,** 24, (2013).
[6]C. Petibois, Anal. Bioanal. Chem., **397,** 2051, (2010).
[7]C. Chen, Y.-F. Li, Y. Qu, Z. Chai, and Y. Zhao, Chem. Soc. Rev. **42,** 8266, (2013).

[8]W. Li, J. O. Tegenfeldt, L. Chen, R. H. Austin, S. Y. Chou, P. A. Kohl, J. Krotine, and J. C. Sturm, Nanotechnology, **14,** 578, (2003).
[9]L. J. Millet and M. U. Gillette, Trends. Neurosci. **35,** 752, (2012).
[10]R. R. Hansen, J. P. Hinestrosa, K. R. Shubert, J. L. Morrell-Falvey, D. A. Pelletier, J. M. Messman, S. M. Kilbey, B. S. Lokitz, and S. T. Retterer, Biomacromolecules. **14,** 3742, (2013).
[11]R. Hansen, K. Shubert, J. Morrell-Falvey, B. Lokitz, M. Doktycz, and S. Retterer, "Microstructured Block Copolymer Surfaces for Control of Microbe Adhesion and Aggregation," Biosensors. **4,** 63, (2014).
[12]L. J. Millet, M. E. Stewart, R. G. Nuzzo, and M. U. Gillette, Lab Chip. **10,** 1525, (2010).
[13]H. Andersson and A. Van den Berg, Sens. Act. B. **92,** 315, (2003).
[14]D. B. Weibel and G. M. Whitesides, Curr. Opin. Chem. Biol. **10,** 584, (2006).
[15]E. Wright, S. Neethirajan, K. Warriner, S. Retterer, and B. Srijanto, Lab Chip. **14,** 938, (2014).
[16]L. J. Millet, M. B. Collens, G. L. W. Perry, and R. Bashir, Integr. Biol. **3,** 1167, (2011).
[17]G. M. Whitesides, Nature. **442,** 368, (2006).
[18]B. P. Helmke and A. R. Minerick, Proc. Natl. Acad. Sci. U.S.A. **103,** 6419, (2006).
[19]M. Zhong, C. Y. Lee, C. A. Croushore, and J. V Sweedler, Lab. Chip. **12,** 2037, (2012).
[20]K. Jo, M. L. Heien, L. B. Thompson, M. Zhong, R. G. Nuzzo, and J. V Sweedler, Lab. Chip. **7,** 1454, (2007).
[21]C. A. Croushore, S. Supharoek, C. Y. Lee, J. Jakmunee, and J. V. Sweedler, Anal. Chem. **84,** 9446, (2012).
[22]H. Parsa, C. D. Chin, P. Mongkolwisetwara, B. W. Lee, J. J. Wang, and S. K. Sia, Lab Chip. **8,** 2062, (2008).
[23]J. Lee, S. A. Soper, and K. K. Murray, Anal. Chim. Acta. **649,** 180, (2009).
[24]S. T. Retterer, P. Siuti, C.-K. Choi, D. K. Thomas, and M. J. Doktycz, Lab Chip. **10,** 1174, (2010).
[25]P. Siuti, S. T. Retterer, C. K. Choi, and M. J. Doktycz, Anal. Chem. **84,** 1092 (2012).
[26]S. T. Retterer, K. L. Smith, C. S. Bjornsson, J. N. Turner, M. S. Isaacson, and W. Shain, J. Neural Eng. **5,** 385, (2008).
[27]S. T. Retterer, K. L. Smith, C. S. Bjornsson, K. B. Neeves, A. J. H. Spence, J. N. Turner, W. Shain, and M. S. Isaacson, IEEE Trans. Biomed. Eng. **51,** 2063, (2004).
[28]E. Abad, A. Juarros, A. Retolaza, S. Merino, R. Marie, and A. Kristensen, Microelectron. Eng. **88,** 300, (2011).
[29]D. Xia, J. Yan, and S. Hou, Small. **8,** 2787, (2012).
[30]N. R. Tas, J. W. Berenschot, P. Mela, H. V. Jansen, M. Elwenspoek, and a. Van Den Berg, "2D-Confined Nanochannels Fabricated by Conventional Micromachining," Nano Lett. **2,** 1031, (2002).
[31]C. Lee, E. E. H. Yang, N. V Myung, and T. George, Nano Lett. **3,** 643, (2003).
[32]L. J. Millet, J. Lucheon, R. F. Standaert, S. T. Retterer, and M. J. Doktycz, Lab Chip. **15,** 1799, 2015.
[33]Y. Yao and A. M. Lenhoff, J. Chromatogr. A **1126,** 107, (2006).
[34]A. Nordborg and E. F. Hilder, Anal. Bioanal. Chem. **394,** 71, (2009).
[35]K. Drescher, Y. Shen, B. Bassler, H. Stone, Proc. Natl. Acad. Sci. U.S.A. **110,** 4345, (2013).

Figures

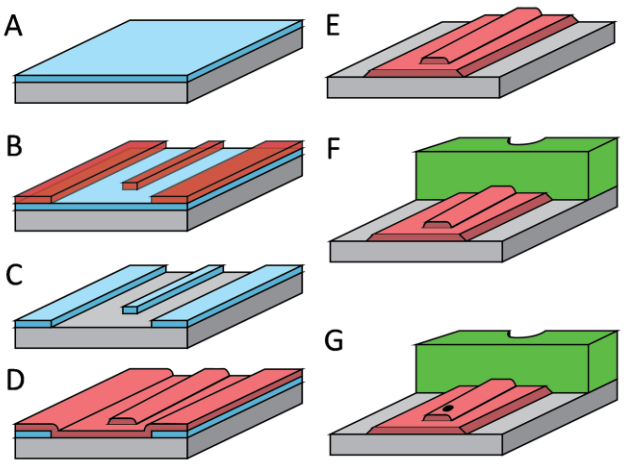

Fig. 1 (Color online). Surface micromachining of nanofluidic interconnects. A) SiO2-coated silicon wafer (<100>, p-type, 500 μm) was used as the starting material. B) Wafer was patterned with electron-beam lithography using ZEP520A resist. C) Pattern was transferred to the SiO_2 layer through RIE. D) Silicon-rich silicon nitride was deposited through PECVD. E) The wafer was exposed to 49% HF (1 min) to remove the sacrificial oxide; the nanochannel surface was retained as the channel interior was cleared of sacrificial oxide and the bulk areas of silicon-nitride were removed. F) SU-8 photopatterning defined the microfluidic architecture. G) Focused-ion-beam was used to mill the channel openings.

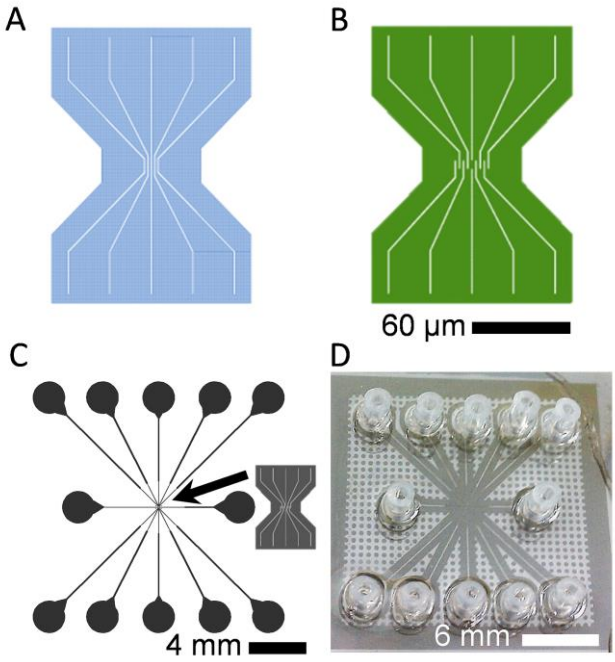

Fig. 2 (Color online). A-B) "Cookie cutter" etch to form two different "bow-tie" nanofluidic architectures for nanofluidic interconnects as a result of the fabrication process (figure 1). The final process is ion milling, or an oxide/nitride etch, to open the channel ends (not show). C) The integrated micro- and nano-fluidic architecture of the entire chip. Two bilateral rows of 5 parallel, circular ports provide access to terminal channels that converge on a single region of nanofluidic channels patterned in bow-tie formation. The two centrally opposing ports that terminate on the ends of the horizontal channel provide access to a single microbial culture channel. D) Completed platforms consist of silicon-nitride nanochannels and SU-8 microfluidics closed with a PDMS membrane integrated with PDMS access tubes.[21] The grid of SU-8 posts inside the square frame provide structural support for the PDMS of the intervening space, this feature enables vacuum-assisted reversible sealing of the PDMS.

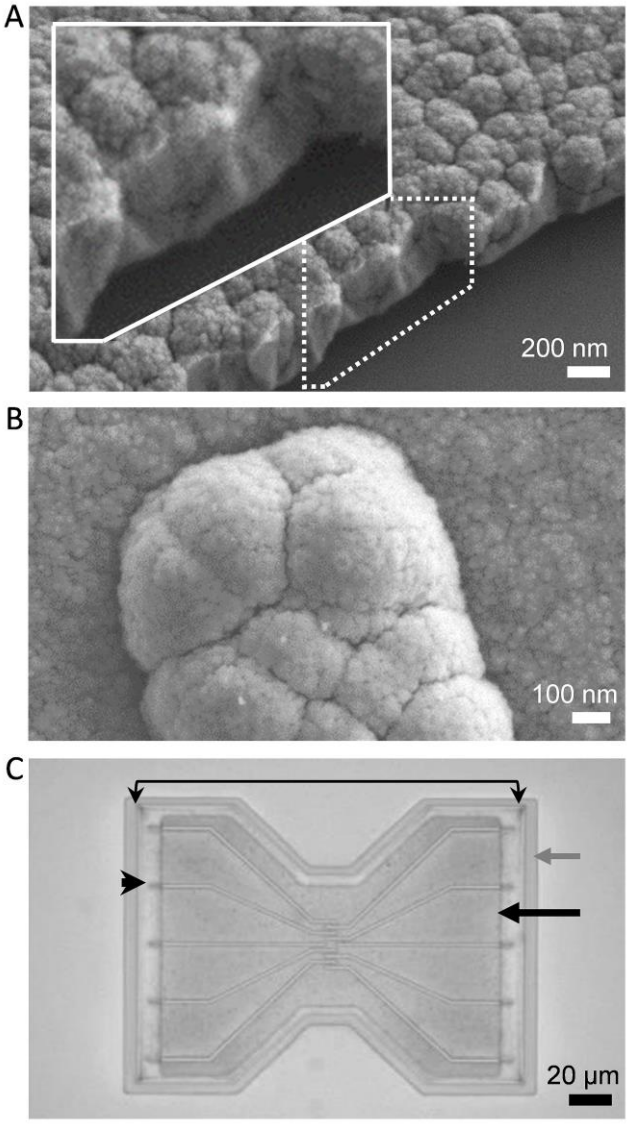

Fig. 3. The silicon-rich silicon nitride (Si_xN_y) deposited on SiO_2 through PECVD creates a semi-porous surface for the nanofluidic architecture. A) SEM side view image of Si_xN_y sheet deposited on SiO_2, inset shows magnified view of silicon-nitride cross-section. B) SEM image of terminal end of a Si_xN_y nanochannel at the center of the bow-tie. Grain size is determined by topology, substrate, and heat conditions during Si_xN_y deposition. C) Optical microscope image of patterned nanochannel array prior to SU-8 photolithography. An area tracing the entire outer edge of the initial EBL pattern (overlapping the ends of the oxide channels) was patterned and etched (RIE) to open the peripheral channel ends (arrow head), creating a small 'bow-tie' (Black arrow) trimmed

away from the edge of the silicon-nitride nanochannel array (grey arrow). For scale, 160 μm between connected arrows.

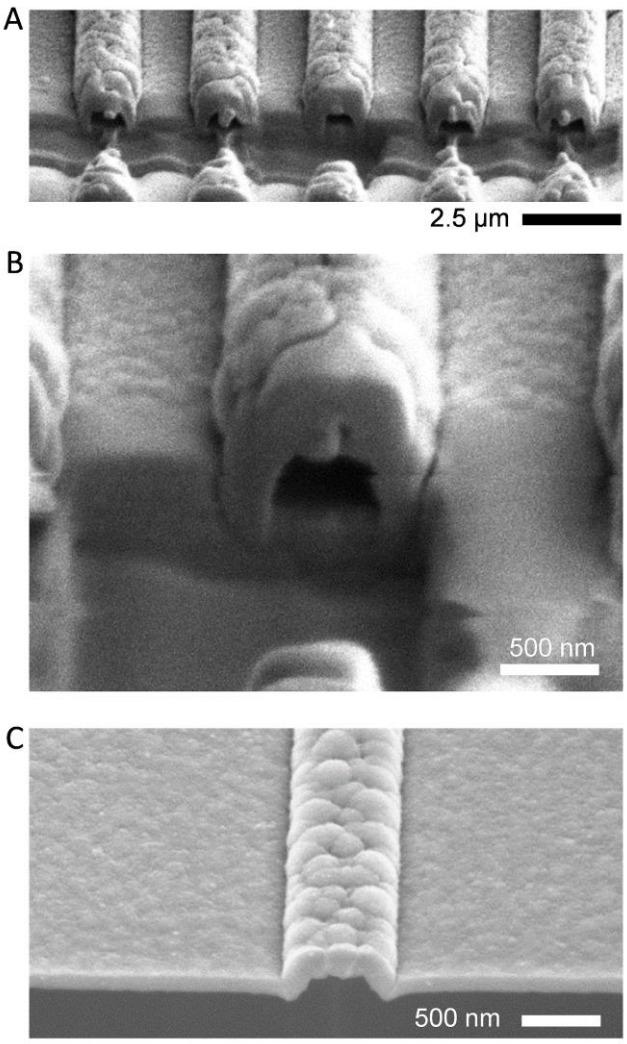

Fig. 4. Clearing out the internal cavity space of closed channels. (A) The HF chemical etch clears the SiO_2 from the internal portion of the nanochannel. (A-B) Ion milling and SEM was used to verify the clearing of the internal portion of the channel as shown. (C) The anisotropic RIE etch process used to perform a "cookie cutter" pattern definition process leaves an overhanging edge that clearly shows the profile of the nanochannel and thickness of the Si_xN_y film.

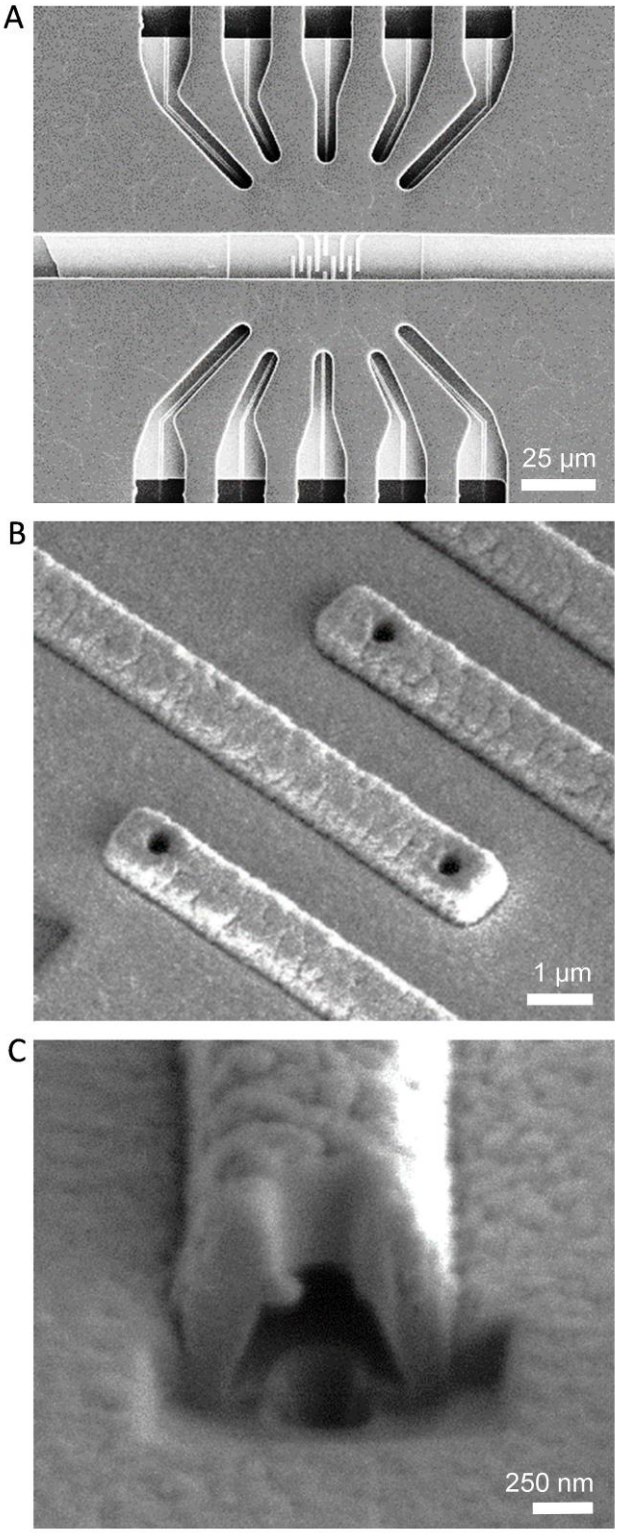

Fig. 5. Nanofluidic interconnects bridging microfluidic domains. A) Lithographically patterned SU-8 microfluidics deposited onto nanochannel bow-tie arrays. (B-C)

Nanochannel openings in the central microfluidic channel are formed with focused-ion beam milling to create perforations for chemical access. (C) SEM of cross-section of ion-milled pore.

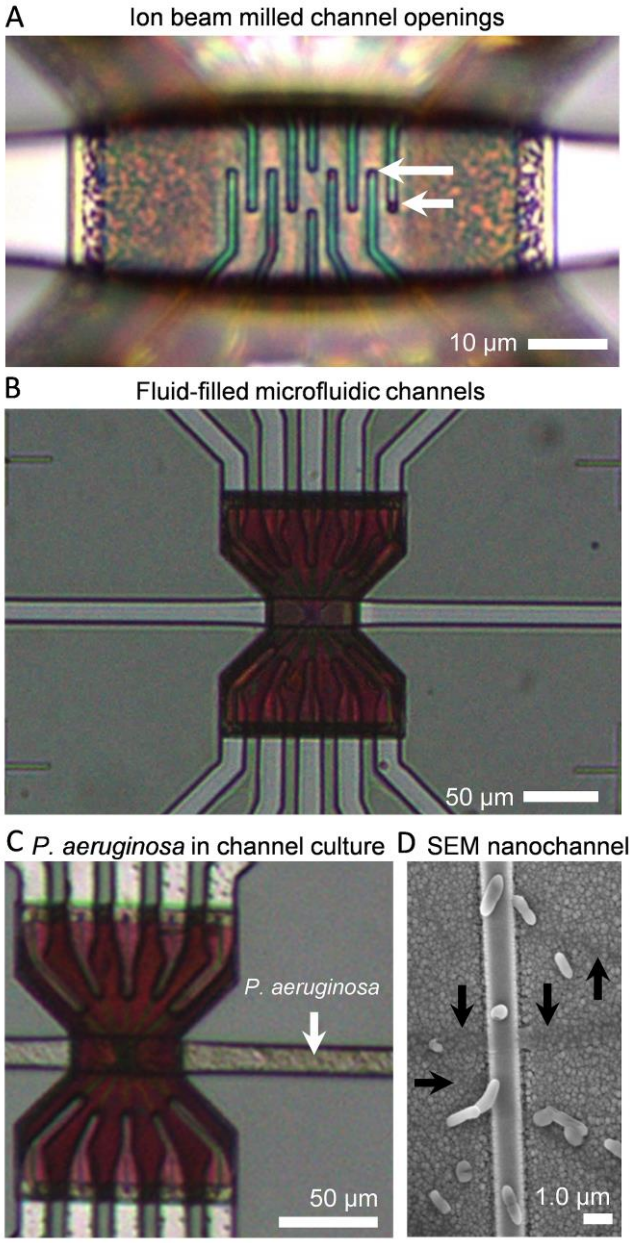

Fig. 6 (Color online). PDMS closure of open SU-8 nanochannels for bacterial cultures. A) Ion-milled nanofluidic channels are observable through conventional optical microscopy; milled channel ends are identified by the black ends (white arrows) of the nanochannels (vertical green interdigitated lines). B) SU-8 microfluidics deposited through photolithography onto nanochannel arrays were sealed with a PDMS closure and filled with saline. Air-plasma exposure and baking of PDMS slabs onto SU-8 provides a tight reversible seal that enables re-opening of the SU-8 channel structures for subsequent analysis. C) Bacterial cultures (*Pseudomonas aeruginosa*) can be cultivated within the

microfluidic channels. PDMS-SU-8 seals provide for microfluidic cultures without PDMS delamination and subsequent leaking into adjacent microfluidic channels; air-filled adjacent channels are identified by 10 white channels. D) Bacterial exopolysaccharide is produced inside the microfluidic culture channel and is observed on the nanochannel surface following chemical fixation and critical point drying.